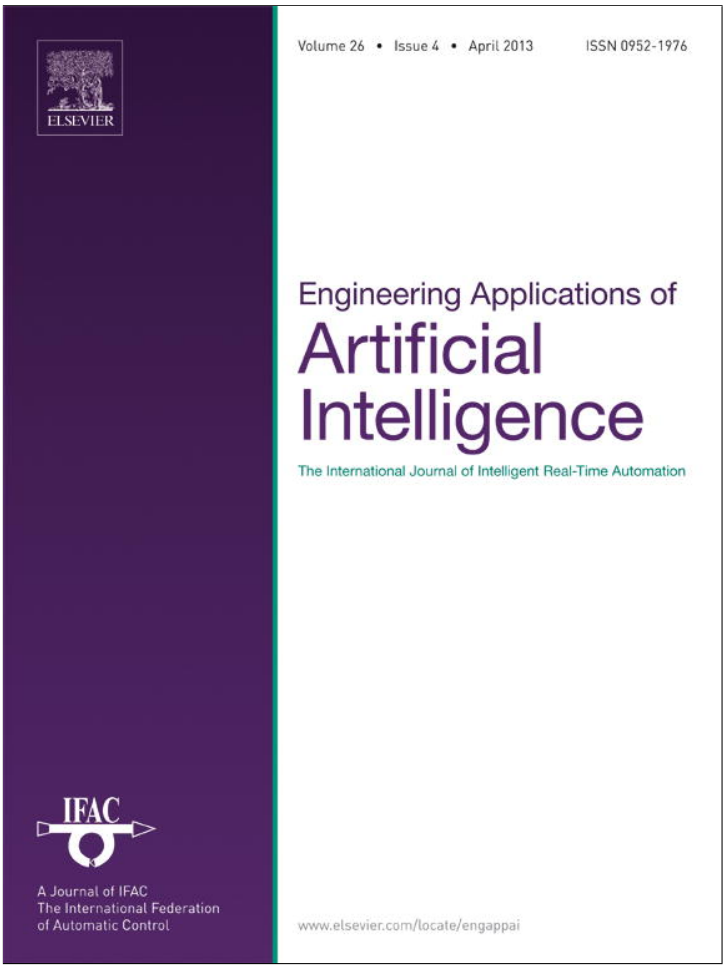

Engineering Applications of Artificial Intelligence 26 (2013) 1221–1229

Contents lists available at SciVerse ScienceDirect

Engineering Applications of Artificial Intelligence

journal homepage: www.elsevier.com/locate/engappai

Adaptive neural complementary sliding-mode control via functional-linked wavelet neural network

Chun-Fei Hsu

Department of Electrical Engineering, Tamkang University, No. 151, Yingzhuan Road, Tamsui District, New Taipei City 25137, Taiwan, Republic of China

ARTICLE INFO

Article history:
Received 26 April 2012
Received in revised form
24 November 2012
Accepted 30 November 2012
Available online 23 December 2012

Keywords:
Adaptive control
Neural control
Functional-linked neural network
Wavelet neural network

ABSTRACT

Chaos control can be applied in the vast areas of physics and engineering systems, but the parameters of chaotic system are inevitably perturbed by external inartificial factors and cannot be exactly known. This paper proposes an adaptive neural complementary sliding-mode control (ANCSC) system, which is composed of a neural controller and a robust compensator, for a chaotic system. The neural controller uses a functional-linked wavelet neural network (FWNN) to approximate an ideal complementary sliding-mode controller. Since the output weights of FWNN are equipped with a functional-linked type form, the FWNN offers good learning accuracy. The robust compensator is designed to eliminate the effect of the approximation error introduced by the neural controller upon the system stability in the Lyapunov sense. Without requiring preliminary offline learning, the parameter learning algorithm can online tune the controller parameters of the proposed ANCSC system to ensure system stable. Finally, it shows by the simulation results that favorable control performance can be achieved for a chaotic system by the proposed ANCSC scheme.

1. Introduction

A model-based non-linear control, which requires a system dynamic of control plants in designing a controller, is an important tool to achieve robust behavior. Since the system may be unknown or perturbed, the model-based non-linear control scheme is difficult to be implemented (Slotine and Li, 1991). In general, a tradeoff problem between the mathematical model accuracy and the control performance arises in a model-based non-linear control system. If all uncertainties existed in the control plants are bounded, a sliding-mode control system provides system dynamics with an invariance property to uncertainties (Utkin, 1978; Wang and Su, 2003). But, high gains are adopted and undesirable chattering phenomenon is resulted to guarantee system stable. The chattering phenomenon becomes the most important disadvantage of a sliding-mode controller. To overcome this problem, an adaptive sliding-mode control with system uncertainties estimator is proposed (Huang et al., 2008). An adaptation law is derived to online estimate the upper bounds of system uncertainties; however, it cannot avoid the estimation growing unboundedly.

Many studies on both the neural networks and fuzzy systems integrating adaptive control techniques have represented an alternative design method for the control of unknown or uncertain non-linear systems (Chen et al., 2009; Chen and Tian, 2009; Chiu, 2010; Czarnigowski, 2010; Huang and Lin, 2011; Hsu, 2012; Li et al., 2007; Zhao and Yu, 2009). The success key element is the self-learning ability that the neural networks and fuzzy systems are used to approximate arbitrary linear or non-linear mappings without requiring preliminary offline tuning. Although the neural networks can learn from data and feedback, the meaning associated with each neuron and each weight in the network is not easily interpreted. Alternatively, the fuzzy systems are easily appreciated because they use linguistic terms and the structure of IF–THEN rules. However, the learning capacity of fuzzy systems is less than that of neural networks.

Recently, neuro-fuzzy networks provide the advantages of both neural networks and fuzzy systems, unlike pure neural networks or fuzzy systems alone. Neuro-fuzzy networks bring the low-level learning and computational power of neural networks into fuzzy systems and give the high-level human-like thinking and reasoning of fuzzy systems to neural networks (Chen, 2009; Elmas et al., 2008; Li and Chen, 2008). In addition, a functional-linked neural network (FLNN) is proposed (Patra and Kot, 2002; Toh and Yau, 2005). The basic idea of FLNN is the use of the functional links. These functional links generate non-linear transformations of the original input space before they are fed into the network which constructs the output layer. The FLNN can approximate a non-linear function effectively since it is able to form the output part of neural network by the non-linear combination of input variables. As a result, there has been

E-mail address: fei@ee.tku.edu.tw

0952-1976/$ - see front matter © 2012 Elsevier Ltd. All rights reserved.
http://dx.doi.org/10.1016/j.engappai.2012.11.012

considerable interest in exploring the applications of FLNN to deal with non-linearities and uncertainties of control system (Chen et al., 2008; Lin et al., 2011).

To achieve better learning performance, some researchers have developed the network structure based on wavelet functions to construct a wavelet neural network (WNN) which absorbs the advantages of wavelet decompositions and learning of neural networks (Billings and Wei, 2005; Chen and Hsu, 2010; Hsu, 2011; Ko, 2012). The wavelet functions have the ability to decompose wideband signals into time and frequency domains simultaneously in order to focus on short time intervals for high-frequency components and on long time intervals for low frequency components. This paper presents a functional-linked wavelet neural network (FWNN) which combines the advantages of the FLNN and WNN. Since the output weights of the proposed FWNN are equipped with a functional-linked type form, the FWNN is used for function approximation with faster convergence rate and less computational loading than a multilayer neural network.

Chaotic system is a non-linear deterministic system that displays complex, noisy-like and unpredictable behavior. It can be observed in many non-linear circuits and mechanical systems (Chen and Dong, 1993). For control engineers, control of a chaotic system has become a significant research topic in physics, mathematics and engineering communities. This paper proposes an adaptive neural complementary sliding-mode control (ANCSC) system which is composed of a neural controller and a robust compensator for a chaotic system. The neural controller uses a FWNN to approximate an ideal complementary sliding-mode controller and the robust compensator is designed to eliminate the effect of the approximation error introduced by the neural controller. The parameter learning algorithm online tune the control parameters based on the gradient descent method and the Lyapunov stability sense. To show the effectiveness of the proposed ANCSC system, a comparison among the complementary sliding-mode control (Wang and Su, 2003), the functional-linked RBF network control (Lin et al., 2011) and the proposed ANCSC is performed. In the simulation study, it is shown that the proposed ANCSC system can achieve better control performance than other methods.

This paper is organized as follows: Section 2 describes the dynamics of a chaotic system and the control problem for chaotic systems is formulated. In Section 3, an ANCSC system is designed with a FWNN. Then, numerical simulations that confirm the validity and feasibility of the proposed method are shown in Section 4. Finally, conclusions are presented in Section 5.

2. Problem statement

Chaotic phenomena have been observed in numerous fields of science such as physics, chemistry, biology and ecology (Chen and Dong, 1993; Lin et al., 2010; Pan et al., 2011; Wu and Bai, 2009). It can be observed in many non-linear circuits and mechanical systems. Consider a second-order chaotic system such as Chen and Dong (1993)

$$\ddot{x} = -p\dot{x} - p_1 x - p_2 x^3 + q\cos(\omega t) + u = f(\mathbf{x}) + u \tag{1}$$

where x is the displacement, $f(\mathbf{x}) = -p\dot{x} - p_1 x - p_2 x^3 + q\cos(\omega t)$ is the system dynamics, t is the time variable, ω is the frequency, u is the control effort, p controls the size of the damping, p_1 controls the size of the restoring force, p_2 controls the amount of non-linearity in the restoring force, q controls the amplitude of the periodic driving force, and ω controls the frequency of the periodic driving force. In this paper, we chose that $p=0.4$, $p_1=-1.1$, $p_2=1.0$, and $\omega=1.8$. Depending on the choices of these constants, the solutions of system (1) may display complex phenomena, including various periodic orbits behaviors and some chaotic behaviors as Chen and Dong (1993). To observe the complex phenomena, the time responses of the uncontrolled chaotic system with initial point (0,0) for $q=2.1$ and $q=7.0$ are shown in Fig. 1(a) and (b), respectively. For the time responses with $q=2.1$, an uncontrolled chaotic trajectory can be found, but a period motion chaotic trajectory happens with $q=7.0$. It is shown that the uncontrolled chaotic system has different trajectories for different system parameters.

The dynamics of a chaotic system are highly time varying and non-linear. The control objective of this paper is to find a control law so that the system state x can track a state command x_c closely. To achieve this control objective, define a tracking error and a sliding surface as Wang and Su (2003)

$$e = x_c - x \tag{2}$$

$$s = \dot{e} + 2ke + k^2 \int_0^t e(\tau)d\tau \tag{3}$$

where k is a positive constant. Next, a complementary sliding surface is designed as Wang and Su (2003)

$$s_c = \dot{e} - k^2 \int_0^t e(\tau)d\tau. \tag{4}$$

A significant result concerning the relationship between s and s_c can be obtained as

$$\dot{s}_c = \dot{s} - k(s + s_c). \tag{5}$$

Differentiating (3) with respect to time and using (1), we can obtain

$$\dot{s} = \ddot{e} + 2k\dot{e} + k^2 e = \ddot{x}_c - f(\mathbf{x}) - u + 2k\dot{e} + k^2 e. \tag{6}$$

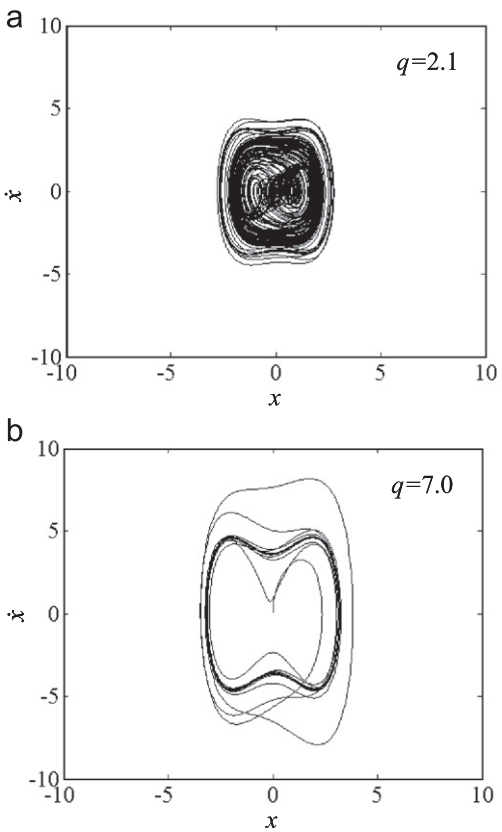

Fig. 1. Behavior of uncontrolled chaotic system.

To design an ideal complementary sliding-mode control law, consider the candidate Lyapunov function in the following form as

$$V_1(s,s_c,t)=\frac{1}{2}s^2+\frac{1}{2}s_c^2. \tag{7}$$

Differentiating (7) with respect to time and using (5) and (6), yields

$$\begin{aligned}\dot{V}_1(s,s_c,t)&=s\dot{s}+s_c\dot{s}_c\\&=s\dot{s}+s_c[\dot{s}-k(s+s_c)]\\&=(s+s_c)(\dot{s}-ks_c)\\&=(s+s_c)[\ddot{x}_c-f(\mathbf{x})-u+2k\dot{e}+k^2e-ks_c].\end{aligned} \tag{8}$$

Assuming that all the parameters in (1) are known, an ideal complementary sliding-mode controller can be given as

$$u^*=\ddot{x}_c-f(\mathbf{x})+k(2\dot{e}+ke+s). \tag{9}$$

Imposing the control law $u=u^*$ in (8) with (9) yields

$$\dot{V}_1(s,s_c,t)=-k(s+s_c)^2\le 0. \tag{10}$$

Since $\dot{V}_1(s,s_c,t)$ is negative semidefinite, that is $V_1(s,s_c,t)\le V_1(s,s_c,0)$, it implies that $s(t)$ and $s_c(t)$ are bounded. Let function $\psi(t)\equiv k(s+s_c)^2\le -\dot{V}_1(s,s_c,t)$ and integrate $\psi(t)$ with respect to time, then it is obtained that

$$\int_0^t\psi(\tau)d\tau\le V_1(s,s_c,0)-V_1(s,s_c,t). \tag{11}$$

Because $V_1(s,s_c,0)$ is bounded and $V_1(s,s_c,t)$ is non-increasing and bounded, the following result obtains

$$\lim_{t\to\infty}\int_0^t\psi(\tau)d\tau<\infty. \tag{12}$$

By Barbalat's Lemma, $\lim_{t\to\infty}\psi(t)=0$. That is $s(t)\to 0$ and $s_c(t)\to 0$ as $t\to\infty$. Then, the stability of the ideal complementary sliding-mode control system can be guaranteed (Slotine and Li, 1991; Wang and Su, 2003).

3. ANCSC system design

The ideal complementary sliding-mode control law in (9) can achieve favorable control performance, but the controller requires the system dynamic of control plants. In the most practical systems, the system dynamic is difficult to develop accurately due to the lack of knowledge of system parameters or external disturbances. To attack this problem, the proposed ANCSC system as shown in Fig. 2 is composed of a neural controller and a robust compensator, i.e.

$$u_{ancs}=u_{nc}+u_{rc} \tag{13}$$

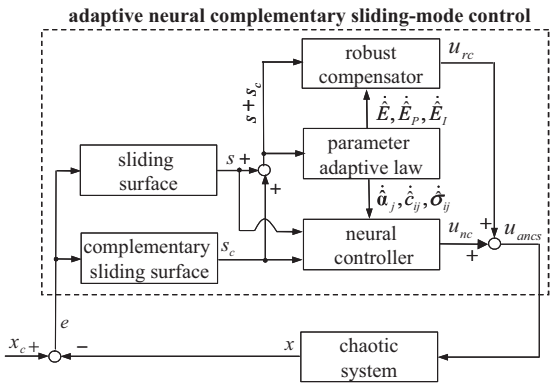

Fig. 2. The block diagram of the ANCSC system.

where the neural controller u_{nc} uses a FWNN to approximate an ideal complementary sliding-mode controller and the robust compensator u_{rc} is designed to eliminate the approximation error between the neural controller and ideal complementary sliding-mode controller. Imposing the control law $u=u_{ancs}$ in (13) with (1) yields

$$\ddot{x}=f(\mathbf{x})+u_{nc}+u_{rc}. \tag{14}$$

The tracking error e is defined in (2), the sliding surface s in (3) and the complementary sliding surface s_c in (4). Using (9) and (14), an error dynamic equation can be obtained as

$$u^*-u_{nc}-u_{rc}-ks=\ddot{e}+2k\dot{e}+k^2e=\dot{s}. \tag{15}$$

3.1. Network structure of FWNN

The network structure of the proposed FWNN as shown in Fig. 3 can be considered as multi-layer feedforward neural network. The operation functions of the nodes in each layer are introduced in the following.

Layer 1: No function is performed in this layer. Each node in this layer only transmits input values x_i $(i=1,2)$ to the next layer directly. In this study, the inputs of FWNN are $x_1=s$ and $x_2=s_c$, which are the sliding surface s in (3) and the complementary sliding surface s_c in (4), respectively.

Layer 2: In this layer, each fuzzy wavelet function can be represented by (Billings and Wei, 2005; Lin, 2006)

$$\varphi_{ij}=h_{ij}\cdot e^{-\sigma_{ij}^2(x_i-c_{ij})^2},\quad \text{for } j=1,2,\ldots,m \tag{16}$$

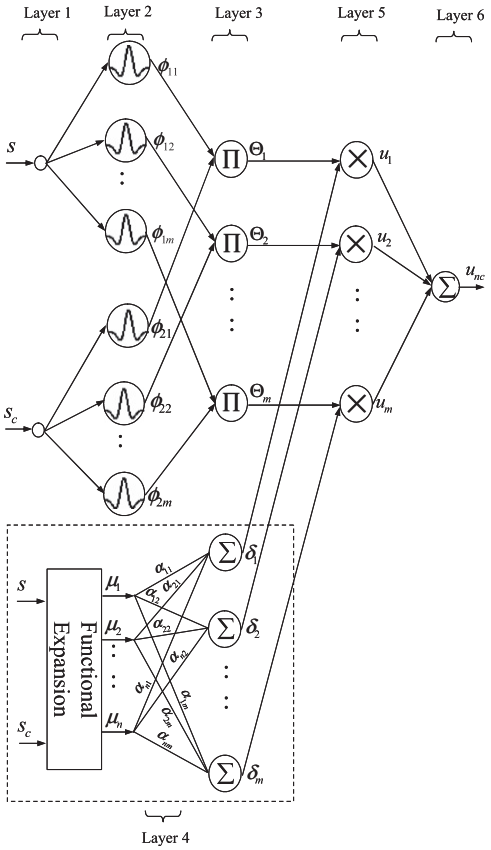

Fig. 3. Network structure of FWNN.

where h_{ij} is the mother wavelet function, σ_{ij} and c_{ij} are the dilation and translation parameters, respectively, m is the number of the fuzzy wavelet function, and each fuzzy wavelet function satisfies that $\int \phi_{ij} dx_i = 0$. In this paper, a "Mexican hat" mother wavelet function is defined as $h_{ij} = 1 - \sigma_{ij}^2 (x_i - c_{ij})^2$ (Lin, 2006).

Layer 3: Nodes in layer 3 receive one-dimensional degrees of the associated hidden neuron from the nodes of a set in layer 2. The output function of each node is given as

$$\Theta_j = \prod_{i=1}^{2} \varphi_{ij}, \quad \text{for } j = 1,2,\ldots,m \tag{17}$$

Layer 4: The input to a node in layer 4 is the output from layer 1. The functional expansion of FLNN acts on each input variable by generating a set of linearly independent functions, and then evaluating these functions with the variables as the arguments. In this study, a trigonometric function is adopted. Consider n orthogonal basis functions as

$$\boldsymbol{\psi} = [\mu_1, \mu_2, \ldots, \mu_n]^T = [x_1, \cos(\pi x_1), \sin(\pi x_1), x_2, \cos(\pi x_2), \sin(\pi x_2)]^T \tag{18}$$

then the output function of each node can perform the mapping according to Chen et al. (2008)

$$\delta_j = \sum_{k=1}^{n} \alpha_{kj} \mu_k = \boldsymbol{\alpha}_j^T \boldsymbol{\psi}, \quad \text{for} \quad j = 1,2,\ldots,m \tag{19}$$

where $\boldsymbol{\alpha}_j = [\alpha_{1j}, \alpha_{2j}, \ldots, \alpha_{nj}]^T$ is the parameter vector specified by designers.

Layer 5: The input to a node in layer 5 is the output from layer 3 and the other input is the output from layer 4. The output function of each node is given as

$$u_j = \delta_j \Theta_j = \boldsymbol{\alpha}_j^T \boldsymbol{\psi} \Theta_j, \quad \text{for} \quad j = 1,2,\ldots,m \tag{20}$$

Layer 6: The output node together with links connected it act. The single node computes the overall output as the summation of all incoming signals. The output of the proposed FWNN can be represented as

$$u_{nc} = \sum_{j=1}^{m} u_j = \sum_{j=1}^{m} \boldsymbol{\alpha}_j^T \boldsymbol{\psi} \Theta_j = \boldsymbol{\alpha}^T \boldsymbol{\Theta} \tag{21}$$

where $\boldsymbol{\alpha} = [\boldsymbol{\alpha}_1^T, \ldots, \boldsymbol{\alpha}_m^T]^T$ and $\boldsymbol{\Theta} = [\Theta_1 \boldsymbol{\psi}^T, \ldots, \Theta_m \boldsymbol{\psi}^T]^T$.

3.2. Stability analysis

The main property of neural network regarding feedback control purpose is the universal function approximation property. It implies that there exists an optimal FWNN such that

$$u^* = \boldsymbol{\alpha}^{*T} \boldsymbol{\Theta} + \varepsilon \tag{22}$$

where $\boldsymbol{\alpha}^*$ is the optimal parameter vector of $\boldsymbol{\alpha}$ and ε denotes the approximation error which is assumed to be bounded by $0 \le |\varepsilon| \le E$ with E as a positive constant. Since the optimal parameter vector is unobtainable to best approximation, a neural controller is defined as

$$u_{nc} = \hat{\boldsymbol{\alpha}}^T \boldsymbol{\Theta} \tag{23}$$

where $\hat{\boldsymbol{\alpha}}$ is the estimated parameter vector of $\boldsymbol{\alpha}$. Substituting (22) and (23) into (15) yields

$$\begin{aligned} \dot{s} &= \boldsymbol{\alpha}^{*T} \boldsymbol{\Theta} - \hat{\boldsymbol{\alpha}}^T \boldsymbol{\Theta} + \varepsilon - u_{rc} - ks \\ &= \tilde{\boldsymbol{\alpha}}^T \boldsymbol{\Theta} + \varepsilon - u_{rc} - ks \end{aligned} \tag{24}$$

where $\tilde{\boldsymbol{\alpha}} = \boldsymbol{\alpha}^* - \hat{\boldsymbol{\alpha}}$. To suppress the influence of the residual approximation error ε, this paper designs the robust compensator as

$$u_{rc} = \begin{cases} \hat{E}_P (s + s_c) + \hat{E}_I \int (s + s_c) dt & \text{for } |s + s_c| \le \Phi \\ \hat{E}\, \mathrm{sgn}(s + s_c) & \text{for } |s + s_c| > \Phi \end{cases} \tag{25}$$

where $\hat{E}$, $\hat{E}_P$ and $\hat{E}_I$ are free controller parameters and Φ is the thickness of the boundary layer. Defined $\hat{\boldsymbol{\varsigma}} = [\hat{E}_P, \hat{E}_I]^T$ and $\boldsymbol{\xi} = [(s + s_c), \int (s + s_c) dt]^T$. When $|s + s_c| \le \Phi$, the robust compensator is defined as $u_{rc} = \hat{\boldsymbol{\varsigma}}^T \boldsymbol{\xi}$, and when $|s + s_c| > \Phi$, the robust compensator is defined as $u_{rc} = \hat{E}\mathrm{sgn}(s + s_c)$. To guarantee the stability of the proposed ANCSC system, two cases are considered separately depending on the value of $|s + s_c|$.

Case 1. For $|s + s_c| > \Phi$, a Lyapunov function is defined as

$$V_2(s, s_c, \tilde{\boldsymbol{\alpha}}, \tilde{E}, t) = \frac{1}{2} s^2 + \frac{1}{2} s_c^2 + \frac{\tilde{\boldsymbol{\alpha}}^T \tilde{\boldsymbol{\alpha}}}{2\eta_\alpha} + \frac{\tilde{E}^2}{2\eta_E} \tag{26}$$

where η_α and η_E are the positive learning rates and $\tilde{E} = E - \hat{E}$. Differentiating (26) with respect to time and using (24) obtain

$$\begin{aligned} \dot{V}_2\left(s, s_c, \tilde{\boldsymbol{\alpha}}, \tilde{E}, t\right) &= s\dot{s} + s_c \dot{s}_c + \frac{\tilde{\boldsymbol{\alpha}}^T \dot{\tilde{\boldsymbol{\alpha}}}}{\eta_\alpha} + \frac{\tilde{E}\dot{\tilde{E}}}{\eta_E} \\ &= (s + s_c)(\dot{s} - k s_c) + \frac{\tilde{\boldsymbol{\alpha}}^T \dot{\tilde{\boldsymbol{\alpha}}}}{\eta_\alpha} + \frac{\tilde{E}\dot{\tilde{E}}}{\eta_E} \\ &= (s + s_c)\left[\tilde{\boldsymbol{\alpha}}^T \boldsymbol{\Theta} + \varepsilon - u_{rc} - k(s + s_c)\right] + \frac{\tilde{\boldsymbol{\alpha}}^T \dot{\tilde{\boldsymbol{\alpha}}}}{\eta_\alpha} + \frac{\tilde{E}\dot{\tilde{E}}}{\eta_E} \\ &= \tilde{\boldsymbol{\alpha}}^T \left[(s + s_c)\boldsymbol{\Theta} + \frac{\dot{\tilde{\boldsymbol{\alpha}}}}{\eta_\alpha}\right] + (s + s_c)(\varepsilon - u_{rc}) - k(s + s_c)^2 + \frac{\tilde{E}\dot{\tilde{E}}}{\eta_E}. \end{aligned} \tag{27}$$

For achieving $\dot{V}_2\left(s, s_c, \tilde{\boldsymbol{\alpha}}, \tilde{E}, t\right) \le 0$, an parameter adaptive law is designed as

$$\dot{\hat{\boldsymbol{\alpha}}} = -\dot{\tilde{\boldsymbol{\alpha}}} = \eta_\alpha (s + s_c)\boldsymbol{\Theta} \tag{28}$$

then (27) can be rewritten as

$$\begin{aligned} \dot{V}_2\left(s, s_c, \tilde{\boldsymbol{\alpha}}, \tilde{E}, t\right) &= (s + s_c)(\varepsilon - u_{rc}) - k(s + s_c)^2 + \frac{\tilde{E}\dot{\tilde{E}}}{\eta_E} \\ &= \varepsilon(s + s_c) - \hat{E}|s + s_c| - k(s + s_c)^2 + \frac{\tilde{E}\dot{\tilde{E}}}{\eta_E} \\ &\le |\varepsilon||s + s_c| - \hat{E}|s + s_c| - k(s + s_c)^2 + \frac{\tilde{E}\dot{\tilde{E}}}{\eta_E} \\ &\le E|s + s_c| - \hat{E}|s + s_c| - k(s + s_c)^2 + \frac{\tilde{E}\dot{\tilde{E}}}{\eta_E} \\ &= \tilde{E}|s + s_c| - k(s + s_c)^2 + \frac{\tilde{E}\dot{\tilde{E}}}{\eta_E} \\ &\le \tilde{E}\left(|s + s_c| + \frac{\dot{\tilde{E}}}{\eta_E}\right) - k(s + s_c)^2. \end{aligned} \tag{29}$$

The bound estimation law is designed as

$$\dot{\hat{E}} = -\dot{\tilde{E}} = \eta_E |s + s_c| \tag{30}$$

then (29) can be obtained

$$\dot{V}_2\left(s, s_c, \tilde{\boldsymbol{\alpha}}, \tilde{E}, t\right) \le -k(s + s_c)^2 \le 0. \tag{31}$$

Similarly to (10), that is $s(t) \to 0$ and $s_c(t) \to 0$ as $t \to \infty$. Then, the stability of the proposed ANCSC system can be guaranteed for $|s + s_c| > \Phi$ (Slotine and Li, 1991; Wang and Su, 2003).

Case 2. For $|s+s_c| \le \Phi$, a Lyapunov function is defined as

$$V_3(s,s_c,\tilde{\boldsymbol{\alpha}},\tilde{\boldsymbol{\xi}},t) = \frac{1}{2}s^2 + \frac{1}{2}s_c^2 + \frac{\tilde{\boldsymbol{\alpha}}^T\tilde{\boldsymbol{\alpha}}}{2\eta_\alpha} + \frac{\tilde{\boldsymbol{\xi}}^T\tilde{\boldsymbol{\xi}}}{2\eta_\xi} \tag{32}$$

where the positive constant η_ξ is the learning rate, $\tilde{\boldsymbol{\xi}} = \boldsymbol{\xi}^* - \hat{\boldsymbol{\xi}}$ and $\boldsymbol{\xi}^*$ is the optimal value for $\boldsymbol{\xi}$ as defined

$$\boldsymbol{\xi}^* = \arg\min_{\boldsymbol{\xi}\in R^2}\left[\sup_{(s+s_c)\in R}|\hat{\boldsymbol{\xi}}^T\boldsymbol{\xi} - E\ \mathrm{sgn}(s+s_c)|\right]. \tag{33}$$

It can be found that $\hat{\boldsymbol{\xi}}^T\boldsymbol{\xi}$ lies in the first and third quadrants and $(s+s_c)\hat{\boldsymbol{\xi}}^T\boldsymbol{\xi} = 0$ for $s+s_c=0$. It concludes that $(s+s_c)\boldsymbol{\xi}^{*T}\boldsymbol{\xi} = |s+s_c||\boldsymbol{\xi}^{*T}\boldsymbol{\xi}|$ and $|\boldsymbol{\xi}^{*T}\boldsymbol{\xi}| \ge E$. Taking the derivative of Lyapunov function (32) and using (24) and (28), yields

$$\begin{aligned}
\dot{V}_3(s,s_c,\tilde{\boldsymbol{\alpha}},\tilde{\boldsymbol{\xi}},t) &= s\dot{s} + s_c\dot{s}_c + \frac{\tilde{\boldsymbol{\alpha}}^T\dot{\tilde{\boldsymbol{\alpha}}}}{\eta_\alpha} + \frac{\tilde{\boldsymbol{\xi}}^T\dot{\tilde{\boldsymbol{\xi}}}}{\eta_\xi} \\
&= (s+s_c)(\dot{s} - k s_c) + \frac{\tilde{\boldsymbol{\alpha}}^T\dot{\tilde{\boldsymbol{\alpha}}}}{\eta_\alpha} + \frac{\tilde{\boldsymbol{\xi}}^T\dot{\tilde{\boldsymbol{\xi}}}}{\eta_\xi} \\
&= \tilde{\boldsymbol{\alpha}}^T\left[(s+s_c)\boldsymbol{\Theta} + \frac{\dot{\tilde{\boldsymbol{\alpha}}}}{\eta_\alpha}\right] + (s+s_c)(\varepsilon - u_{rc}) - k(s+s_c)^2 + \frac{\tilde{\boldsymbol{\xi}}^T\dot{\tilde{\boldsymbol{\xi}}}}{\eta_\xi} \\
&= (s+s_c)\left(\varepsilon - \hat{\boldsymbol{\xi}}^T\boldsymbol{\xi}\right) - k(s+s_c)^2 + \frac{\tilde{\boldsymbol{\xi}}^T\dot{\tilde{\boldsymbol{\xi}}}}{\eta_\xi} \\
&= (s+s_c)\left(\varepsilon - \hat{\boldsymbol{\xi}}^T\boldsymbol{\xi} + \boldsymbol{\xi}^{*T}\boldsymbol{\xi} - \boldsymbol{\xi}^{*T}\boldsymbol{\xi}\right) - k(s+s_c)^2 + \frac{\tilde{\boldsymbol{\xi}}^T\dot{\tilde{\boldsymbol{\xi}}}}{\eta_\xi} \\
&= (s+s_c)\left(\varepsilon + \tilde{\boldsymbol{\xi}}^T\boldsymbol{\xi} - \boldsymbol{\xi}^{*T}\boldsymbol{\xi}\right) - k(s+s_c)^2 + \frac{\tilde{\boldsymbol{\xi}}^T\dot{\tilde{\boldsymbol{\xi}}}}{\eta_\xi} \\
&= \tilde{\boldsymbol{\xi}}^T\left[(s+s_c)\boldsymbol{\xi} + \frac{\dot{\tilde{\boldsymbol{\xi}}}}{\eta_\xi}\right] + (s+s_c)(\varepsilon - \boldsymbol{\xi}^{*T}\boldsymbol{\xi}) - k(s+s_c)^2.
\end{aligned} \tag{34}$$

If the adaptation laws is chosen as

$$\dot{\tilde{\boldsymbol{\xi}}} = -\dot{\hat{\boldsymbol{\xi}}} = \eta_\xi(s+s_c)\boldsymbol{\xi} \tag{35}$$

then (34) can be rewritten as

$$\begin{aligned}
\dot{V}_3(s,s_c,\tilde{\boldsymbol{\alpha}},\tilde{\boldsymbol{\xi}},t) &= (s+s_c)(\varepsilon - \boldsymbol{\xi}^{*T}\boldsymbol{\xi}) - k(s+s_c)^2 \\
&\le |\varepsilon||s+s_c| - |\boldsymbol{\xi}^{*T}\boldsymbol{\xi}||s+s_c| - k(s+s_c)^2 \\
&\le |\varepsilon||s+s_c| - E|s+s_c| - k(s+s_c)^2 \\
&= -(E-|\varepsilon|)|s+s_c| - k(s+s_c)^2 \\
&\le -k(s+s_c)^2 \le 0.
\end{aligned} \tag{36}$$

Similarly to (10), that is $s(t)\to 0$ and $s_c(t)\to 0$ as $t\to\infty$. Then, the stability of the proposed ANCSC system can be guaranteed for $|s+s_c| \le \Phi$ (Slotine and Li, 1991; Wang and Su, 2003).

3.3. Full parameter learning

In order to describe the online training algorithm of FWNN, a cost function is defined as

$$C = \frac{1}{2}e^2. \tag{37}$$

According to the gradient descent method, the adaptive law of the controller parameters can be represented as (Lin and Lee, 1996)

$$\dot{\boldsymbol{\alpha}}_j = -\eta_\alpha\frac{\partial C}{\partial \boldsymbol{\alpha}_j} = -\eta_\alpha\frac{\partial C}{\partial u_{nc}}\frac{\partial u_{nc}}{\partial \boldsymbol{\alpha}_j} = -\eta_\alpha\frac{\partial C}{\partial u_{nc}}\Theta_j\boldsymbol{\psi}^T. \tag{38}$$

If the plant dynamics is unknown, the Jacobian term $\partial C/\partial u_{nc}$ cannot be obtained in advance. Therefore, the updating rule cannot work properly during the learning process. Comparing (28) with (38), the Jacobian term of the system can be found as $\partial C/\partial u_{nc} = -(s+s_c)$ in this study. Then, the adaptation laws of two adjustable parameters (c_{ij} and σ_{ij}) can be derived via the gradient descent method to increase the learning capability, i.e.

$$\begin{aligned}
\dot{c}_{ij} &= -\eta_c\frac{\partial C}{\partial c_{ij}} = -\eta_c\frac{\partial C}{\partial u_{nc}}\frac{\partial u_{nc}}{\partial \Theta_j}\frac{\partial \Theta_j}{\partial \varphi_{ij}}\frac{\partial \varphi_{ij}}{\partial c_{ij}} \\
&= 2\eta_c(s+s_c)\boldsymbol{\alpha}_j^T\boldsymbol{\psi}\Theta_j\sigma_{ij}^2(x_i - c_{ij})
\end{aligned} \tag{39}$$

$$\begin{aligned}
\dot{\sigma}_{ij} &= -\eta_\sigma\frac{\partial C}{\partial \sigma_{ij}} = -\eta_\sigma\frac{\partial C}{\partial u_{nc}}\frac{\partial u_{nc}}{\partial \Theta_j}\frac{\partial \Theta_j}{\partial \varphi_{ij}}\frac{\partial \varphi_{ij}}{\partial \sigma_{ij}} \\
&= -2\eta_\sigma(s+s_c)\boldsymbol{\alpha}_j^T\boldsymbol{\psi}\Theta_j\sigma_{ij}(x_i - c_{ij})^2
\end{aligned} \tag{40}$$

where η_c and η_σ are positive learning rates.

4. Simulation and experimental results

It should be emphasized that the development of the proposed ANCSC system does not need to know the mathematical model of control plants. For practical implementation, the controller parameters can be online tuned by the proposed learning algorithm. To illustrate the effectiveness of the proposed ANCSC system, a comparison among the complementary sliding-mode control (CSMC) (Wang and Su, 2003), the functional-linked RBF network control (Lin et al., 2011) and the proposed ANCSC is performed. In all simulations, the step time used to control the system is 0.002 s.

First, the CSMC system (Wang and Su, 2003) is applied to control a chaotic system. It is known that the major advantage of the CSMC system is its insensitivity to parameter variations and external disturbance once the system trajectory reaches and stays on the sliding surface (Slotine and Li, 1991). An important concept is to make the system satisfy the reaching condition and guarantee sliding condition. A conservative control law which requires the bound of the system uncertainty is usually considered. The simulation results of the CSMC system with small uncertainty bound for $q=2.1$ and $q=7.0$ are shown in Figs. 4 and 5, respectively. The tracking responses of state x are shown in Figs. 4(a) and 5(a), the tracking responses of state $\dot{x}$ are shown in Figs. 4(b) and 5(b), the control inputs are shown in Figs. 4(c) and 5(c), and the tracking errors are shown in Figs. 4(d) and 5(d). The simulation results show that favorable control performance can be achieved for $q=2.1$ but it cannot for $q=7.0$. Since a not sufficiently large uncertainty bound is chosen, the states of the controlled system does not enter the sliding mode for $q=7.0$. Thus, the degenerate tracking response is resulted and the undesirable chattering phenomenon does not appear. Furthermore, the CSMC system with large uncertainty bound is applied to control a chaotic system again. The simulation results of the CSMC system with large uncertainty bound for $q=2.1$ and $q=7.0$ are shown in Figs. 6 and 7, respectively. The tracking responses of state x are shown in Figs. 6(a) and 7(a), the tracking responses of state $\dot{x}$ are shown in Figs. 6(b) and 7(b), the control inputs are shown in Figs. 6(c) and 7(c), and the tracking errors are shown in Figs. 6(d) and 7(d). Though satisfied control performance can be achieved for $q=2.1$ and $q=7.0$, the undesirable chattering phenomenon occurs as shown in Figs. 6(c) and 7(c). A trade-off problem between chattering and control accuracy arises in the CSMC scheme.

Then, the functional-linked RBF network control system (Lin et al., 2011) is applied to control a chaotic system again. The simulation results of the functional-linked RBF network control for $q=2.1$ and $q=7.0$ are shown in Figs. 8 and 9, respectively. The tracking responses of state x are shown in Figs. 8(a) and 9(a), the tracking responses of state $\dot{x}$ are shown in Figs. 8(b) and 9(b), the control inputs are shown in Figs. 8(c) and 9(c), and the

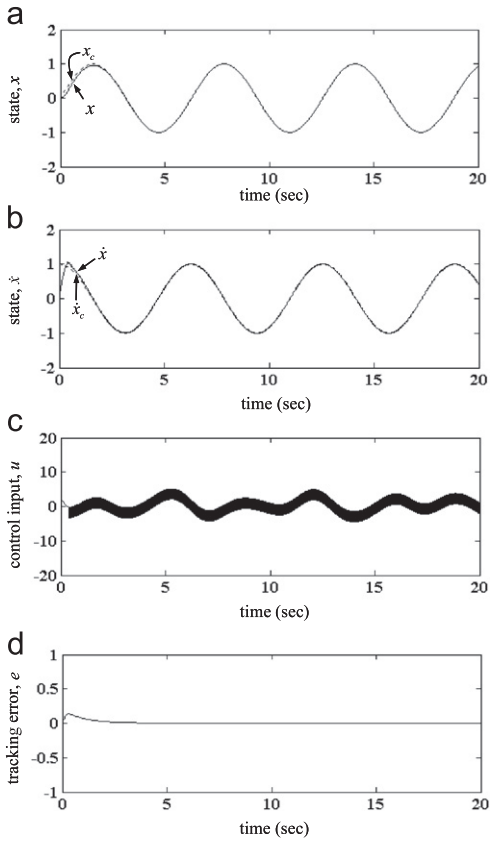

Fig. 4. Simulation results of the CSMC system with small uncertainty bound for $q=2.1$.

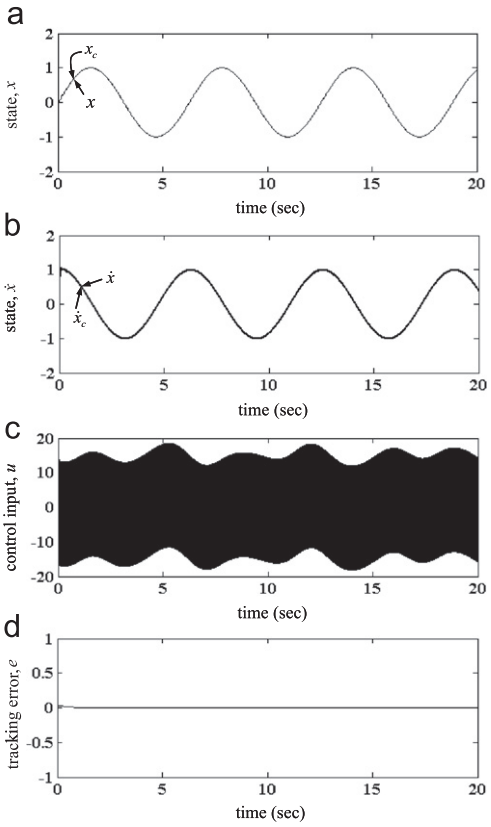

Fig. 6. Simulation results of the CSMC system with large uncertainty bound for $q=2.1$.

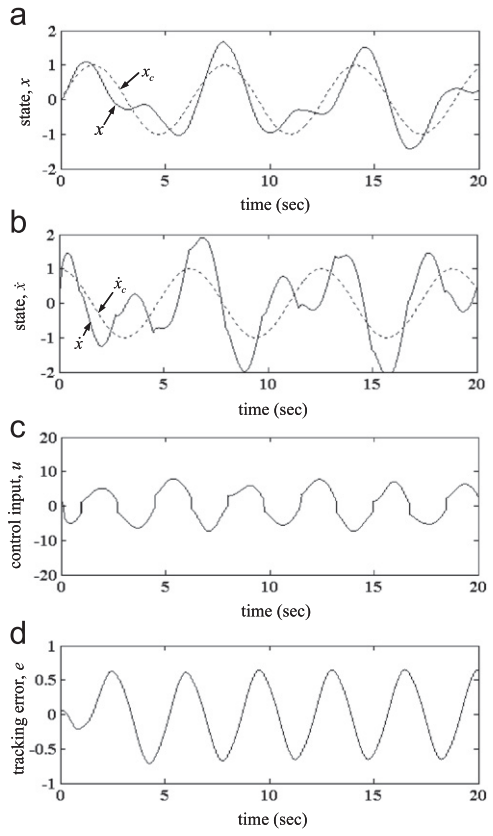

Fig. 5. Simulation results of the CSMC system with small uncertainty bound for $q=7.0$.

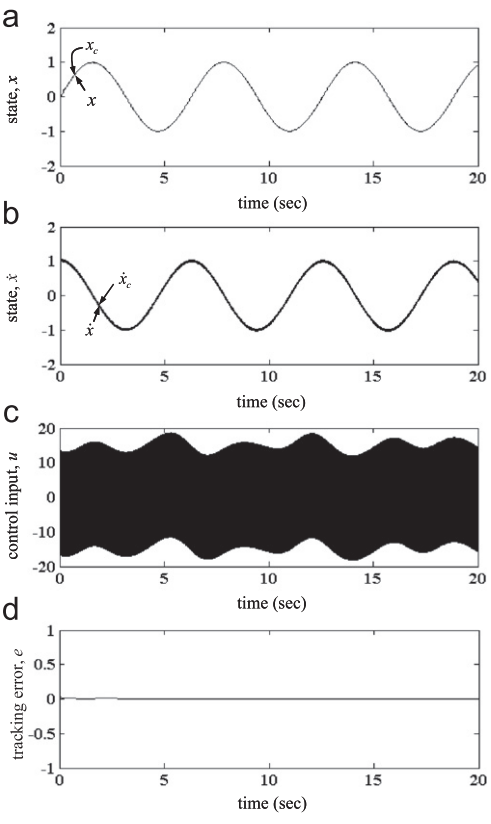

Fig. 7. Simulation results of the CSMC system with large uncertainty bound for $q=7.0$.

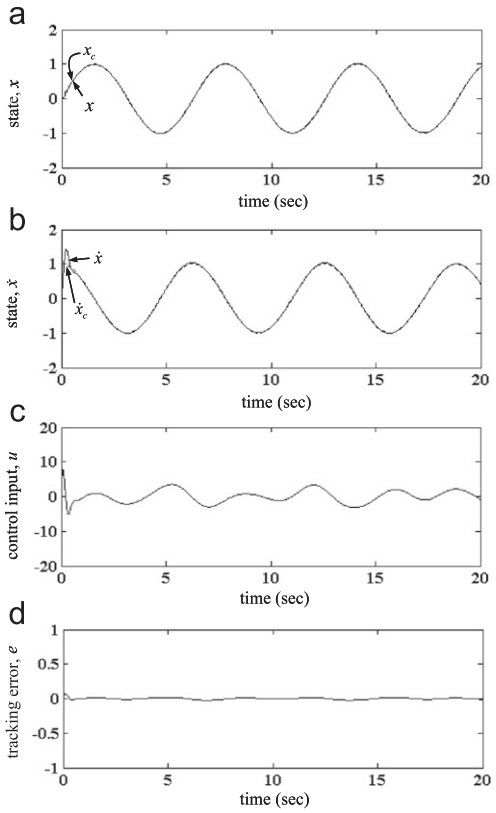

Fig. 8. Simulation results of the functional-linked RBF network control for $q=2.1$.

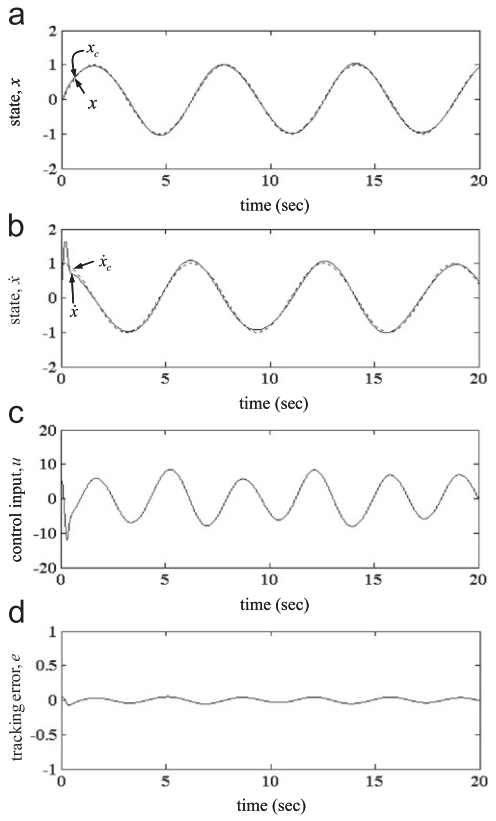

Fig. 9. Simulation results of the functional-linked RBF network control for $q=7.0$.

tracking errors are shown in Figs. 8(d) and 9(d). The simulation results show that the functional-linked RBF network control system can achieve favorable tracking performance even under the variations of system parameters. But, the paper does not consider the influence of the residual approximation error introduced by the functional-linked RBF network.

Finally, the proposed ANCSC system is applied to control a chaotic system again. The parameters of the ANCSC system are selected as $\eta_\alpha=0.1$, $\eta_c=\eta_\sigma=0.01$, $\eta_E=\eta_\varsigma=1$, and $k=1$. The choices of these values are through some trials considering the requirement of stability condition. The parameters η_α, η_c and η_σ are the leaning rates of the neural controller and the parameters η_E and η_ς are the leaning rate of the robust compensator. If the leaning rates are chosen small, the parameter convergence will be easily achieved; however, this will result in slow learning speed. On the other hand, if the leaning rates are chosen large, the learning speed will be fast; however, the system may become unstable. The simulation results of the ANCSC system for $q=2.1$ and $q=7.0$ are shown in Figs. 10 and 11, respectively. The tracking responses of state x are shown in Figs. 10(a) and 11(a), the tracking responses of state $\dot{x}$ are shown in Figs. 10(b) and 11(b), the control inputs are shown in Figs. 10(c) and 11(c), and the tracking errors are shown in Figs. 10(d) and 11(d). The simulation results show that a satisfied tracking performance can be achieved after the controller parameters learning even under the variations of system parameters. However, since the parameter vectors of FWNN are initialized from zero, the ANCSC system has the drawback of large transient responses of the state trajectories at the initial learning phase. After 20 s training in these simulations, the trained ANCSC system is applied to control a chaotic system again. The simulation results of the trained ANCSC system for $q=2.1$ and $q=7.0$ are shown in Figs. 12 and 13, respectively. The tracking responses of state x are shown in Figs. 12(a) and 13(a), the tracking responses of state $\dot{x}$ are shown in Figs. 12(b) and 13(b), the control inputs are shown in Figs. 12(c) and 13(c), and the tracking errors are shown in

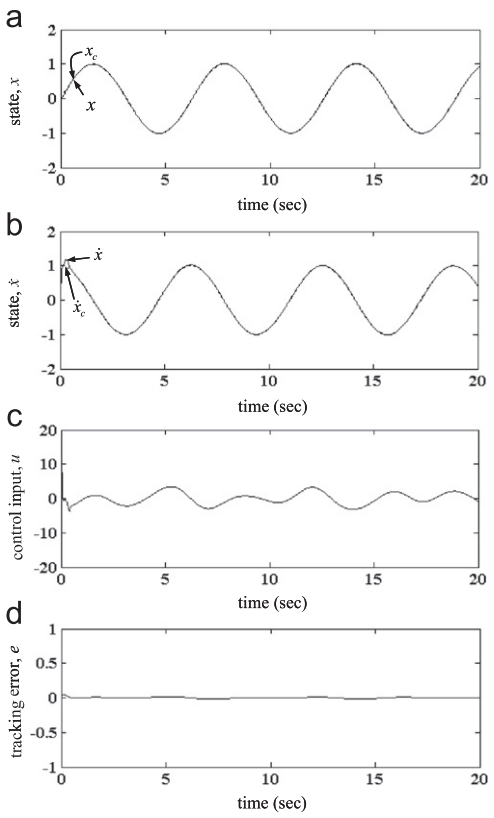

Fig. 10. Simulation results of the ANCSC system for $q=2.1$.

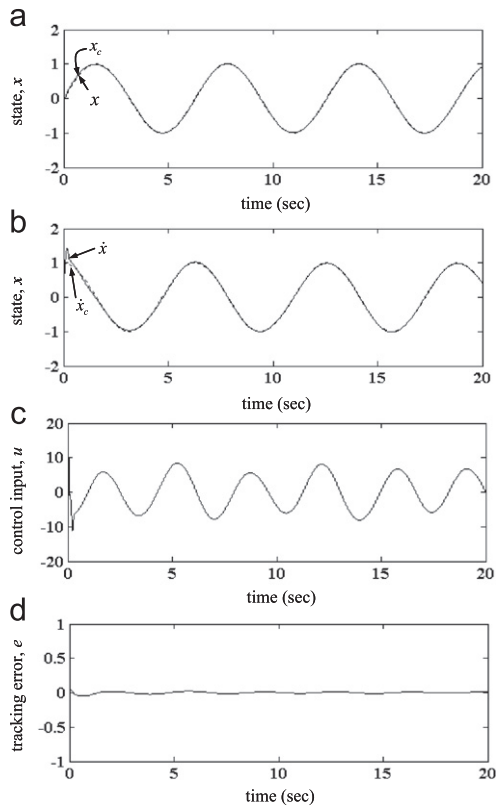

Fig. 11. Simulation results of the ANCSC system for $q=7.0$.

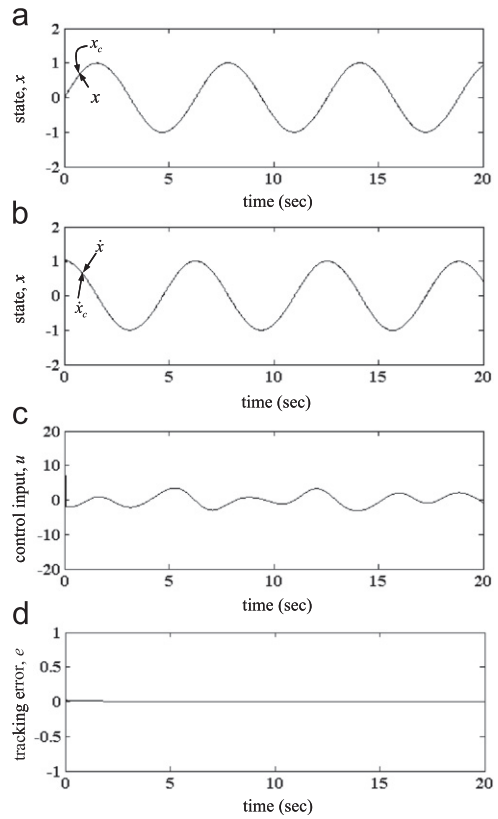

Fig. 12. Simulation results of the trained ANCSC system for $q=2.1$.

Figs. 12(d) and 13(d). From these simulation results, it shows that the tracking performance of the trained ANCSC system is better than other methods.

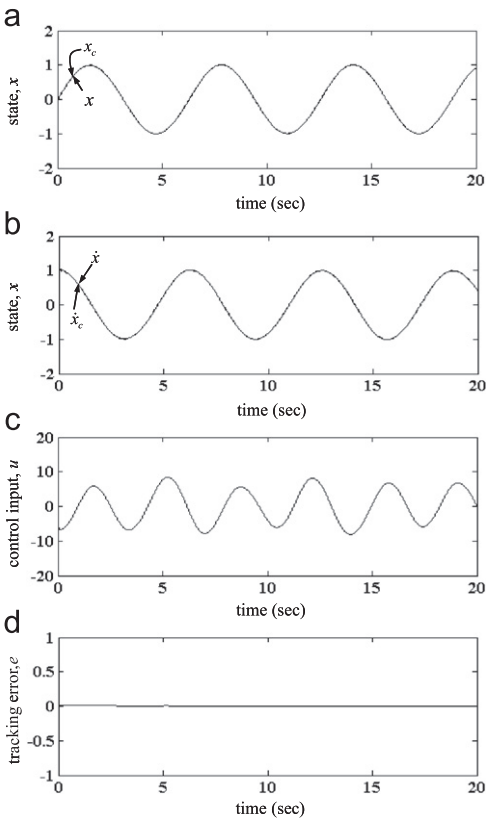

Fig. 13. Simulation results of the trained ANCSC system for $q=7.0$.

In summary, the performance measures of various control systems for the chaotic system are summarized in Table 1 and the comparison of controller characteristics is performed in Table 2. It shows that the proposed ANCSC system possesses the most accurate tracking performance and the proposed ANCSC system is more suitable for the chaotic system.

5. Conclusions

This paper has been successfully developed an adaptive neural complementary sliding-mode control (ANCSC) system which is composed of a neural controller and a robust compensator. The neural controller uses a functional-linked wavelet neural network (FWNN) to approximate an ideal complementary sliding-mode controller and the robust compensator is designed to eliminate the effect of the approximation error introduced by the neural controller. The major contributions of this paper are (1) the successful development of a FWNN with faster convergence rate and less computational loading. (2) The successful development of the ANCSC system. The parameter learning algorithm is design based on the gradient descent method and the Lyapunov stability sense. (3) The robust compensator is proposed to remove the chattering phenomena in the control input. (4) The successful applications of the ANCSC system to control a second-order chaotic system. Further works on the proposed ANCSC design include (1) auto-tuning of the learning rates in the adaptive laws can be considered to increase the convergence of the controller parameters, and (2) MIMO non-linear control problem liking as wheeled mobile manipulators and Tennessee Eastman challenge process (Li and Kang, 2010; Li et al., 2010; Zerkaoui. et al., 2009) can be considered.

Table 1
Performance measures.

Methods	Tracking Error					
	$q=2.1$			$q=7.0$		
	Maximum	Average	Standard Deviation	Maximum	Average	Standard Deviation
CSMC with small uncertainty bound	0.1398	0.0096	0.0247	0.7118	0.3814	0.2083
CSMC with large uncertainty bound	0.0271	0.0027	0.0036	0.0218	0.0050	0.0029
Functional-linked RBF network control	0.0681	0.0096	0.0077	0.0730	0.0277	0.0146
ANCSC	0.0464	0.0061	0.0059	0.0343	0.0082	0.0064
Trained ANCSC	0.0186	0.0023	0.0028	0.0160	0.0039	0.0024

Table 2
Comparison of controller characteristics.

Controller	Controller parameters	Stability proof	Robustness	Chattering phenomena
CSMC with small uncertainty bound	Trial and error	yes	Poor	yes
CSMC with large uncertainty bound	Trial and error	yes	Excellent	yes
Functional-linked RBF network control	On-line learning	no	Middle	no
ANCSC	On-line learning	yes	Excellent	no
Trained ANCSC	On-line learning	yes	Excellent	no

Acknowledgments

The authors are grateful to the reviewers for their valuable comments. The authors appreciate the partial financial support from the National Science Council of Republic of China under the grant NSC 100-2628-E-032-003.

References

Billings, S.A., Wei, H.L., 2005. A new class of wavelet networks for nonlinear system identification. IEEE Trans. Neural Netw. 16, 862–874.
Chen, C.H., Hsu, C.F., 2010. Recurrent wavelet neural backstepping controller design with a smooth compensator. Neural Computing Appl. 19, 1089–1100.
Chen, C.H., Lin, C.J., Lin, C.T., 2008. A functional-link-based neuro-fuzzy network for nonlinear system control. IEEE Trans. Fuzzy Syst. 16, 1362–1378.
Chen, C.S., 2009. Dynamic structure adaptive neural fuzzy control for MIMO uncertain nonlinear systems. Inf. Sci. 179, 2676–2688.
Chen, G., Dong, X., 1993. On feedback control of chaotic continuous-time systems. IEEE Trans. Circuits Syst. 40 (Pt-1), 591–601.
Chen, P.C., Hsu, C.F., Lee, T.T., Wang, C.H., 2009. Fuzzy-identification-based adaptive backstepping control using a self-organizing fuzzy system. Soft Comput. 13, 635–647.
Chen, W., Tian, Y.P., 2009. Neural network approximation for periodically disturbed functions and applications to control design. Neurocomputing 72, 3891–3900.
Chiu, C.H., 2010. The design and implementation of a wheeled inverted pendulum using an adaptive output recurrent cerebellar model articulation controller. IEEE Trans. Ind. Electron 57, 1814–1822.
Czarnigowski, J., 2010. A neural network model-based observer for idle speed control of ignition in SI engine. Eng. Appl. Artif. Intell. 23, 1–7.
Elmas, C., Ustun, O., Sayan, H.H., 2008. A neuro-fuzzy controller for speed control of a permanent magnet synchronous motor drive. Expert Syst. Appl. 34, 657–664.
Huang, C.H., Lin, C.L., 2011. Evolutionary neural networks and DNA computing algorithms for dual-axis motion control. Eng. Appl. Artif. Intell. 24, 1263–1273.
Huang, Y.J., Kuo, T.C., Chang, S.H., 2008. Adaptive sliding-mode control for nonlinear systems with uncertain parameters. IEEE Trans. Syst. Man Cybern. 38 (Pt-B), 534–539.
Hsu, C.F., 2011. Adaptive fuzzy wavelet neural controller design for chaos synchronization. Expert Syst. Appl. 38, 10475–10483.
Hsu, C.F., 2012. Adaptive dynamic CMAC neural control of nonlinear chaotic systems with L_2 tracking performance. Eng. Appl. Artif. Intell. 25, 997–1008.
Ko, C.N., 2012. Identification of nonlinear systems with outliers using wavelet neural networks based on annealing dynamical learning algorithm. Eng. Appl. Artif. Intell. 25, 533–543.
Li, Z., Yang, C., Gu, J., 2007. Neuro-adaptive compliant force/motion control of uncertain constrained wheeled mobile manipulator. Int. J. Robot Autom. 22, 206–214.
Li, Z., Chen, W., 2008. Adaptive neural-fuzzy control of uncertain constrained multiple coordinated nonholonomic mobile manipulators. Eng. Appl. Artif. Intell. 21, 985–1000.
Li, Z., Kang, Y., 2010. Dynamic coupling switching control incorporating support vector machines for wheeled mobile manipulators with hybrid joints. Automatica 46, 832–842.
Li, Z., Li, J., Kang, Y., 2010. Adaptive robust coordinated control of multiple mobile manipulators interacting with rigid environments. Automatica 46, 2028–2034.
Lin, C.K., 2006. Nonsingular terminal sliding mode control of robot manipulators using fuzzy wavelet networks. IEEE Trans. Fuzzy Syst. 14, 849–859.
Lin, C.M., Lin, M.H., Peng, Y.F., 2010. Synchronization of chaotic gyro systems using recurrent wavelet CMAC. Cybern. Syst. 41, 391–405.
Lin, C.T., Lee, C.S.G., 1996. Neural Fuzzy Systems: A Neuro-Fuzzy Synergism to Intelligent Systems. Prentice-Hall, Englewood Cliffs, NJ.
Lin, F.J., Hsieh, H.J., Chou, P.H., Lin, Y.S., 2011. Digital signal processor-based cross-coupled synchronous control of dual linear motors via functional link radial basis function network. IET Control Theory and Appl. 5, 552–564.
Pan, Y., Er., M.J., Huang, D., Wang, Q., 2011. Fire-rule-based direct adaptive type-2 fuzzy H^{∞} tracking control. Eng. Appl. Artif. Intell. 24, 1174–1185.
Patra, J.C., Kot, A.C., 2002. Nonlinear dynamic system identification using Chebyshev functional link artificial neural networks. IEEE Trans. Syst. Man Cybern. 32 (Pt-B), 505–511.
Slotine, J.J.E., Li, W.P., 1991. Applied Nonlinear Control. Prentice-Hall, Englewood Cliffs, NJ.
Toh, K.A., Yau, W.Y., 2005. Fingerprint and speaker verification decisions fusion using a functional link network. IEEE Trans. Syst. Man Cybern. 35 (Pt-C), 357–370.
Utkin, V.I., 1978. Sliding Modes and Theirs Applications in Variable Structure Systems. MIR Editors, Moscow.
Wang, C.C., Su, J.P., 2003. Composite sliding mode control of chaotic systems with uncertainties. I. J. Bifurcation and Chaos 13, 863–878.
Wu, H.N., Bai, M.Z., 2009. Active fault-tolerant fuzzy control design of nonlinear model tracking with application to chaotic systems. IET Control Theory and Appl. 3, 642–653.
Zerkaoui, S., Druaux, F., Leclercq, E., Lefebvre, D., 2009. Stable adaptive control with recurrent neural networks for square MIMO non-linear systems. Eng. Appl. Artif. Intell. 22, 702–717.
Zhao, Y.J., Yu, D.L., 2009. Neural network model-based automotive engine air/fuel ratio control and robustness evaluation. Eng. Appl. Artif. Intell. 22, 171–180.